CO_2 Coordination to Nickel Atoms: Matrix Isolation and Density Functional Studies

F. Galan, M. Fouassier, M. Tranquille, and J. Mascetti*

Laboratoire de Spectroscopie Moléculaire et Cristalline, Université Bordeaux I, 351, cours de la Libération, 33405 Talence Cedex, France

I. Pápai*

Institute of Isotopes of the Hungarian Academy of Sciences, Spectroscopy Department, P.O.B. 77, H-1525 Budapest, Hungary

Received: January 9, 1997[⊗]

The interaction of the CO_2 molecule with nickel atoms was studied by using matrix isolation spectroscopy and density functional theory. In argon dilute matrices, no reaction occurs, even after annealing the deposit. In neat CO_2 matrices, it is shown that carbon dioxide forms a 1:1 complex with nickel which is characterized by its UV−visible and FTIR absorptions, including isotopically labeled species. Theory predicts the side-on coordination mode to be the most stable. The binding energy of the side-on Ni(CO_2) complex is estimated to be 18 kcal/mol. The calculated OCO angle is 145°, which is quite a large value compared to those encountered in other known CO_2 complexes. In dinitrogen matrices, the yield of CO_2 complexation is considerably enhanced relative to that in argon dilute and neat CO_2 matrices, which is attributed to the formation of unsaturated Ni$(N_2)_n$ complexes prior to CO_2 coordination. The CO_2 binding energies calculated for the Ni$(CO_2)(N_2)_n$ ($n = 1, 2$) complexes (respectively 32 and 4 kcal/mol) suggest that CO_2 probably coordinates to the Ni(N_2) complex. This is a very interesting result, owing to the fact that CO_2 does not react with nickel atoms in dilute argon matrices.

I. Introduction

The chemical reactivity of atoms with small molecules is a very active area of research, both experimentally and theoretically. The reactions of transition metal atoms with carbon dioxide are particularly important because this molecule is a potential alternative precursor in organic synthesis, provided that new ways are found to activate it. Activation of carbon dioxide may be accomplished photochemically, electrochemically, or catalytically but, in all cases, the coordination of CO_2 on the metallic center seems to be the key step for the ultimate reduction of CO_2.[1] For this purpose, we previously reported the first systematic study of M(CO_2) (M = Ti, V, Cr, Fe, Ni, Co, Cu) molecules, which was performed, using FTIR matrix isolation spectroscopy in neat CO_2 matrices,[2] in order to understand the nature of the bonding, the most stable geometry, and the common features and differences among these species.

In spite of the large quantities of CO_2 available, only a few processes using it as a raw material have been developed by the synthetic chemical industry.[3,4] One of the most promising routes to the reduction of CO_2 to organic acids, carbonates, peroxocarbonates or carbamates uses nickel catalysts, but the intermediate species formed during the reactions are still unknown. Thus, we decided to reinvestigate the nickel/CO_2 system. The main features of the current study are the use of FTIR to investigate isotopically labeled species: Ni($^{13}CO_2$), Ni($C^{18}O_2$), the use of Ni/CO_2/Ar concentration and annealing effects on the FTIR and UV−visible spectra, the use of normal coordinate analysis of $NiCO_2$, and the use of N_2 matrices.

Results obtained from density functional theory (DFT) calculations on the Ni(CO_2) compound and two different mixed CO_2/N_2 complexes are also reported in this paper, which were performed at a level of the theory that has recently been applied to a number of transition metal−monoligand systems.[5] One of the general conclusions emerging from these studies is that the predicted vibrational frequencies, especially those calculated with nonlocal functionals, are quite accurate; their absolute error is typically within ±50 cm^{-1}. In the present work, DFT is used to determine the mode of coordination of the CO_2 molecule in the complex, to predict the equilibrium properties of the identified species, to describe the bonding in it, and finally to rationalize the enhanced yield of CO_2 complexation in the presence of N_2 molecules.

The paper is organized as follows. In the two first sections, we describe the experimental and the computational conditions used. The species observed, both in argon and dinitrogen matrices, are presented in the third section and characterized by their electronic and vibrational spectra, including isotopically labeled species ($^{13}CO_2$, $C^{18}O_2$). The next section gives the theoretical results obtained by density functional calculations. The experimental and theoretical results are then discussed in terms of the mode of coordination and bonding in the metallic CO_2 complexes incorporating the results of the normal coordinate analysis. Matrix effects on metal/molecule reactivity are also discussed.

II. Experimental Section

The furnace for metal vaporization and the remainder of the apparatus have been described previously.[6,7] Atoms were generated by directly heating a thin ribbon of nickel, strung between two water-cooled electrodes.

Nickel was supplied by Goodfellow Metals (99.98%). CO_2 (99.995%), Ar (99.9995%), and N_2 (99.998%) were supplied by Air Liquide and used without further purification. In addition to $^{12}C^{16}O_2$, isotopically substituted carbon dioxide $^{13}C^{16}O_2$ (99.5% enriched) and $^{12}C^{18}O_2$ (97% enriched), provided by Euriso-Top, were used to identify reaction products and assign vibrational bands.

* To whom correspondence should be addressed.
⊗ Abstract published in *Advance ACS Abstracts,* March 1, 1997.

S1089-5639(97)00155-2 CCC: $14.00 © 1997 American Chemical Society

TABLE 1: Total Energies (E_{total}, hartree) and Zero Point Vibrational Energies (E_{ZPE}, kcal/mol) of the Ground States of the Investigated Systems[a]

	multiplicity	E_{total}	E_{ZPE}
$Ni(CO_2)$[b]	1	−1696.8851	7.2
$Ni(N_2)$	1	−1617.8247	4.6
$Ni(N_2)_2$	1	−1727.4194	9.0
$Ni(CO_2)(N_2)$	1	−1806.4820	12.6
$Ni(CO_2)(N_2)_2$	1	−1916.0313	17.2
CO_2	1	−188.6046	7.1
N_2	1	−109.5275	3.3
Ni (^{3}D, s^1d^9) atom[c]	3	−1508.2467	

[a] The equilibrium geometries of the CO_2 complexes are given in Table 4; the optimized structures (all linear) for the rest of the molecules are as follows: $Ni(N_2)$ R(NiN) = 1.674, R(NN) = 1.143 Å; $Ni(N_2)_2$ R(NiN) = 1.750, R(NN) = 1.132 Å; CO_2 R(CO) = 1.177 Å; N_2 R(NN) = 1.118 Å. [b] The most stable isomer. [c] The lowest lying nonspherical (i.e., integer orbital occupations) solution.

The matrix molar ratios were M/gas = 1/1000. The metal deposition rate was continuously controlled by using a quartz crystal microbalance. Nickel and gases were cocondensed at 1 mmol/h for 2−4-h periods. Matrices were deposited on CsBr windows cooled to 12 K by means of a Cryophysics closed cycle refrigerator Cryodine M22.

Infrared spectra were recorded with a Bruker 113V interferometer, at a resolution of 2 cm^{-1}. UV−visible spectra were recorded on the same samples, using a PU8700 spectrometer with a resolution of 2 nm.

III. Computational Details

The quantum chemical calculations were carried out within the LCGTO-DF formalism[8−12] using the deMon program.[13−15] All properties of the investigated molecules have been obtained at the nonlocal level of theory, using the B-P86 functional (Becke's[16] nonlocal corrections to the Dirac−Slater local spin density (LSD) exchange term[17] and Perdew's[18] nonlocal correlation functional from 1986).

All-electron orbital basis sets were employed for all atoms with contraction patterns (63311/5211/41) for nickel[19] and (5211/411/1) for carbon[20] and oxygen[20] atoms. The corresponding auxiliary basis sets, used in fitting the charge density and the exchange-correlation potential, have the patterns (5,5;5,5)[19] and (5,2;5,2),[20] respectively. The applied numerical quadrature grid has been described in ref 21.

The geometries of the molecules were fully optimized without symmetry constraint and Pulay's force method[22] was applied to construct the cartesian force constant matrix, which was then diagonalized to get the normal frequencies and normal vectors. The IR intensities were calculated from numerical derivatives of the dipole moment vector by using the double harmonic approximation.[23] The displacement of the Cartesian coordinates in the finite-difference procedures was always 0.01 au.

The binding energies will be reported with respect to the ground state (^{3}D, s^1d^9) nickel atom and the geometry optimized ground state ligands (CO_2 and N_2). The binding energies and the reaction energies were always corrected for the zero point energy (ZPE) contributions estimated from the calculated harmonic frequencies. However, they were not corrected for the basis set superposition error (BSSE), unless stated otherwise in the text. The total energies and the ZPE's of the ground states of the investigated systems are listed in Table 1.

The program used to calculate the generalized valence force field in normal coordinate analysis was a modified version of Schachtschneider's.[24] All modes were calculated by using internal coordinates, but because the available experimental data were limited, the fitting was restricted to the five planar modes, the total number of nonzero interaction force constants being three.

In the refinement procedure, the adjustment of the isotopic shifts had priority over that of frequencies because the former are more sensitive to the geometry of the molecule. The initial force field was taken from values previously calculated for the complex $(PCy_3)_2Ni(CO_2)$.[25]

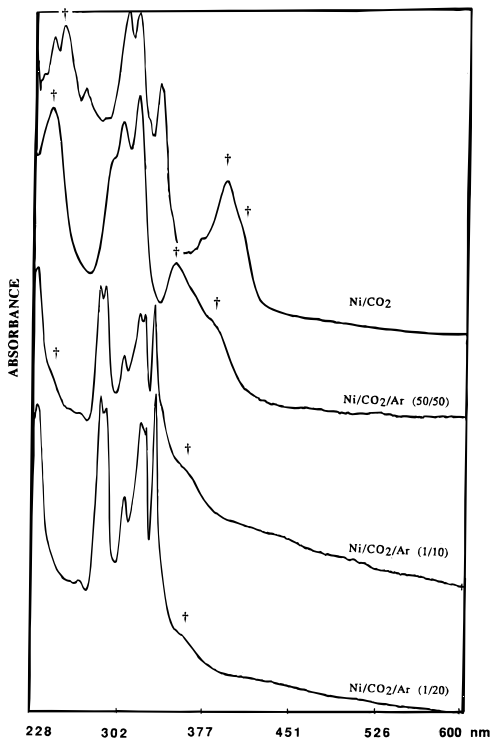

Figure 1. Effect of CO_2 concentration on the UV−visible spectra (λ in nm) of $Ni/CO_2/Ar$ matrices at 10 K.

IV. Experimental Results

IV.1. Experimental Results in CO_2/Ar and Neat CO_2 Matrices. *IV.1.1. UV−Visible Spectra.* In argon matrices, the main d-d transitions of the nickel atoms are located at 230, 280, 300, 320, and 330 nm.[26] Schroeder et al. have shown[26] that nickel atoms exist in Ar matrices in two different electronic states: a stable one, $^3D_3$ (s^1d^9), and a thermally unstable one, $^3F_4$ (s^2d^8), which disappears above 30 K.

Figure 1 shows the CO_2/Ar concentration effect on the UV−visible spectra of $Ni/CO_2/Ar$ deposits. For the most dilute matrices (CO_2/Ar = 1/20 and 1/10), one can observe the main electronic transitions of nickel atoms at 230(s) nm ($^3F_4$) and 283(s), 289(sh), 305(w), 318(s), 323(sh), and 331(s) nm ($^3D_3$), together with weak shoulders at 242 and 346 nm. The UV−visible spectrum recorded for nickel atoms condensed in a more concentrated matrix (CO_2/Ar = 1/1) shows that these shoulders are now medium bands located at 242(s) and 349(m) nm, with a shoulder at 382 nm. The central part of the spectrum consists in three broad bands at 293(sh), 303(s), and 316(s) nm. Finally, in neat CO_2 matrix, the spectrum exhibits absorptions at 251-(br), 306(s), 315(s), and 336(m) nm, together with a broad band at 394(ms) nm and a shoulder at 406 nm.

In annealing experiments with dilute deposits, the $^3F_4$ nickel atoms bands vanished at 25 K and all other bands progressively disappeared by 35 K. No increase of the shoulders at 242 and 346 nm was discerned. In neat carbon dioxide deposits, all bands progressively decreased by annealing up to 80 K and new broad bands at 220, 265, and 300(sh) nm appeared and persisted up to 106 K, which is the sublimation temperature of the CO_2 matrix.

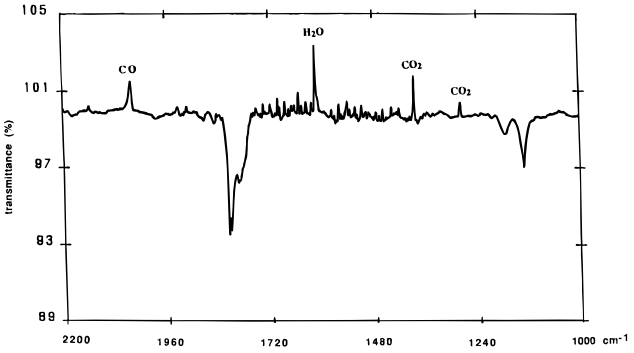

Figure 2. FTIR spectrum (ν in cm^{-1}) of Ni/CO_2 (1/1000) matrix at 10 K.

Since the absorptions at 293, 303, and 316 nm (in concentrated CO_2/Ar matrices) and at 306, 315, and 336 nm (in neat CO_2) show only a slight shift from the atomic absorptions of the nickel, they correspond to transitions of "naked" nickel atoms, weakly interacting with surrounding CO_2 molecules. The bands at 242, 349, 382 nm (in concentrated CO_2/Ar matrices) and at 251, 394, 406 nm (in neat CO_2) can be attributed to the formation of $Ni(CO_2)_n$ species. There is no indication of the formation of nickel aggregates, as no absorption was detected in the 400−600 nm range.[27]

IV.1.2. Infrared Spectra. Similar behavior was observed with FTIR spectroscopy: no absorption bands, except those of free CO_2, were detected in spectra of dilute argon matrices.

For CO_2/Ar = 1/1 deposits, no signal was obtained at 12 K, but a weak broad mutiplet appeared in the region of carbonyl stretching vibrations after annealing to 23K: 1844(sh), 1838, 1820, 1808(sh), 1789(sh), and 1778 cm^{-1}. Further annealing led to progressive vanishing of the spectrum except for the 1844-cm^{-1} band. After evaporation of argon above 40 K, only two bands remained at 1996 and 1844 cm^{-1}. In addition, bands located at 2140 cm^{-1}, due to free carbon monoxide, and at 2042, 1934, and 1914 cm^{-1}, due to CO_2 aggregates, grew during the annealing process.

Figure 2 shows the infrared spectrum of nickel atoms condensed in a neat CO_2 matrix: it consists of a set of bands located at 1850(sh), 1818(s), 1812(s), and 1794(sh) cm^{-1}, together with four other weak absorptions at 1170(w), 1131-(m), 750(sh), and 744(w) cm^{-1}. This spectrum remained unchanged up to 106 K, the sublimation point of the CO_2 matrix. At this temperature, two very broad bands appeared at 2050 and 750 cm^{-1}, which can be respectively assigned to carbonyl ν(CO) and metal oxide ν(NiO) stretching modes. From the profiles of these bands, which are sharp for those at 1818, 1812, 1131, and 744 cm^{-1} and broad for those at 1850, 1794, 1170, and 750 cm^{-1}, it is obvious that two different $Ni(CO_2)_n$ complexes (respectively A and B) exist in the matrix, the second one (B) being less abundant and not well isolated.

IV.1.3. Isotopic Effects. The FTIR spectrum of $Ni/^{13}CO_2$ deposit shows, besides free $^{13}CO_2$ absorptions, three bands in the carbonyl stretching region located at 1802(s), 1773(s), and 1752(w) cm^{-1}, two bands in the C−O stretching area at 1154-(br) and 1116(m) cm^{-1}, and a weak band at 730 cm^{-1} in the OCO bending mode region. These bands are easily correlated with those previously observed in nonlabeled matrices: 1815 (which is the average value of the 1818, 1812 cm^{-1} doublet), 1131, and 744 cm^{-1} are respectively shifted by 42, 15, and 14 cm^{-1}, whereas weaker and broader absorptions at 1850, 1794, and 1170 cm^{-1} are respectively shifted by 48, 42, and 16 cm^{-1}.

Experiments with $C^{18}O_2$, although they led to spectra of poorer quality, gave similar results with a set of bands at 1803, 1775, and 1747 cm^{-1}, leading to isotopic shifts of 47, 40, and 47 cm^{-1} for the three ν(C═O) modes observed in neat CO_2 matrices. For the ν(CO) modes, it was difficult to determine where the two absorptions at 1170 and 1131 cm^{-1} were shifted, but two weak broad bands were detected at 1149 and 1113 cm^{-1}, inducing isotopic shifts of 21 and 18 cm^{-1}, whereas the OCO bending vibration was shifted by 28 cm^{-1} to 716 cm^{-1}.

Similar experiment with a mixture of $C^{16}O_2/C^{18}O_2$ led to a spectrum with a quadruplet at 1812, 1771, 1792, and 1752 cm^{-1}, showing that the $Ni(CO_2)_n$ complexes formed have a 1:1 stoichiometry. In this region, after annealing at 106 K, one doublet appeared at 2050, 2035 cm^{-1} and another doublet was observed at 758 and 738 cm^{-1}, which gave evidence for the reduction of CO_2 to CO, as we previously described[2] with nonlabeled compounds. The spectrum was less clear in the ν-(C-O) region, where a broad absorption was observed between 1170 and 1113 cm^{-1}.

These results are listed in Table 2 and discussed in section VI.

TABLE 2: Tentative Assignment of Observed Wavenumbers (cm^{-1}) in FTIR Spectra of Ni Deposits in Neat CO_2, $^{13}CO_2$, $C^{18}O_2$, and Diluted CO_2/N_2 (1/10) Matrices at 10K

Ni/CO_2	$Ni/^{13}CO_2$	$Ni/C^{18}O_2$	$Ni/CO_2/N_2$	assignment[a]
			2220(w)[b,c]	ν(NN)
			2172(vs)[b]	ν(NN), $Ni(N_2)_4$
			2166(vs)[b]	ν(NN), $Ni(N_2)_4$
			2118(m)[c]	
			2098(m)[c]	
			2060(s)	ν(NN), C
			1901(sh)	
			1895(sh)	
			1884(s)	ν(C═O), C
			1863(sh)[c]	
			1851(s)	ν(C═O), D
1850(sh)	1802	1803		ν(C═O)
1815(s)	1773	1775		ν(C═O), A
1794(sh)	1752	1747	1792(w)	ν(C═O), B
1170(w)	1154	1149		ν(CO), B
			1151(ms)	ν(CO), C
1131(m)	1116	1113		ν(CO), A
			1096(m)	ν(CO), D
750(w)				δ(OCO), B
744(m)	730	716		δ(OCO), A
			725(m)	δ(OCO), C
			708(sh)	δ(OCO), D
			561(w)[b]	ν(NiN)
			514(w)	γ(C═O), C
			486(w)[b,c]	ν(NiN)
410(w)	400	410		ν(NiO), A
			399(w)[b,c]	ν(NiN)
			281(s)[b]	ν(NiN), $Ni(N_2)_4$
			270(w)[b,c]	δ(NiNN)

[a] A, B, C, D: see text. [b] Also observed in Ni/N_2 deposits. [c] Grows by annealing.

IV.2. Exprimental Results in CO_2/N_2 Matrices. In order to compare the reactivity of nickel atoms toward carbon dioxide in different media, we decided to study condensation experiments in dinitrogen matrices (concentration ratio: CO_2/N_2 = 1/10).

The reactivity of N_2 toward nickel atoms was already studied[28,29] and four $Ni(N_2)_n$ complexes have been described with n = 1−4 and characterized by their infrared and Raman spectra.

The electronic spectrum of $Ni/CO_2/N_2$ matrix at 10 K shows that all of the nickel atoms are complexed, most of them being coordinated to N_2 molecules to form the saturated complex $Ni(N_2)_4$, which absorbs at 247 nm.[6b] This strong, broad band has a shoulder at 354 nm that might arise from a species involving coordinated CO_2. The spectrum remains unchanged to 40 K. No signal due to nickel aggregates was detected.[27]

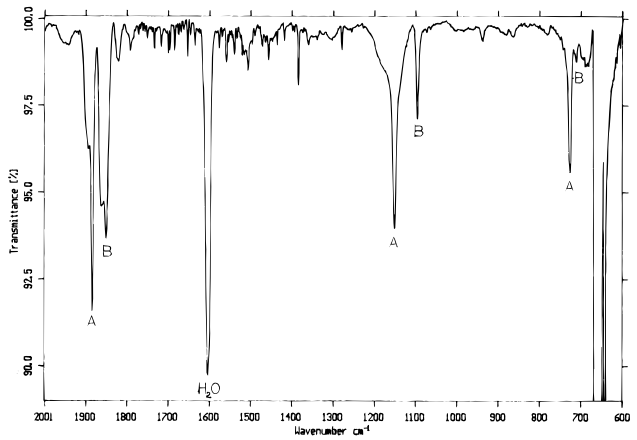

Figure 3. FTIR spectrum (ν in cm^{-1}) of $Ni/CO_2/N_2$ matrix at 10 K (Ni/matrix = 1/1000, CO_2/N_2 = 1/10).

As expected, the FTIR spectrum of the deposit (Figure 3) is dominated by the strong absorptions of $Ni(N_2)_4$ at 2172, 2166, and 281 cm^{-1}, but additional bands appear in the ν(NN), ν(C═O), ν(CO), δ(OCO), and low frequency regions. These bands can be divided in two groups, depending on their behavior during annealing experiments: 2060(m), 1901(sh), 1895(sh), 1884(s), 1851(m), 1792(w, br), 1151(m), 1096(m), 725(m), 708(w), 561(w), and 514(w) cm^{-1} decrease and 2220(w), 2118(w), 2098(w), 1863(m), 1822(vw), 486(w), 399(w), and 270(w) cm^{-1} increase during annealing of the matrix. All the bands vanish above 45 K, except for $Ni(N_2)_4$ and two new absorptions at 1996 and 1944 cm^{-1}. Dinitrogen has a phase transition at 35 K, above which temperature it is no longer a good matrix medium:[30] so that nickel atoms are found to aggregate and broad bands are observed on FTIR spectra.

Unlike with $Ni/CO_2/Ar$ matrices, the presence of bands in the CO stretching region implies the formation of CO_2 complexes in $Ni/CO_2/N_2$ deposits. As already observed for systems such as $Li/C_2H_4/N_2/Ar$,[31] the presence of dinitrogen promotes the coordination of carbon dioxide to nickel atoms. Further experiments, including concentration effects and isotopic labeling, must be undertaken to fully characterize the species formed, but a simple comparison of the spectrum with those obtained in neat CO_2 allows us to propose an assignment summarized in Table 2. On the basis of the band intensities, the absorptions at 2060, 1884, 1151, 725, 561 cm^{-1} and 1851, 1096, 708, 514 cm^{-1} can be associated to two different mixed nickel/CO_2/N_2 complexes (respectively C and D).

Among the other complexes formed in the matrix, we probably have bridged species, such as $Ni_x(N_2)_n$, $Ni_x(CO)_p$, or $Ni_x(N_2)_n(CO)_p$, as no nickel aggregates were detected in electronic spectra and no absorption could be assigned to monometallic terminal carbonyl complexes $Ni(CO)_n$ (n = 1−4),[32] mixed compounds $Ni(CO)_n(N_2)_{4-n}$,[33] or nickel surface species.[34]

V. Theoretical Results

V.1. The $Ni(CO_2)$ Complex. The CO_2 molecule can coordinate to a single transition metal atom in one of four different modes (Figure 4). We carried out geometry optimization for the singlet and triplet states of all four isomers and calculated the harmonic vibrational frequencies and IR intensities at their equilibrium geometries. The obtained results are given in Table 3.

The singlet η^2_{CO} is found to be the most stable form, all other structures lie at least 15 kcal/mol higher in energy. Most of the structures found in the geometry optimization are minima on the potential energy surface (PES); however, the singlet states

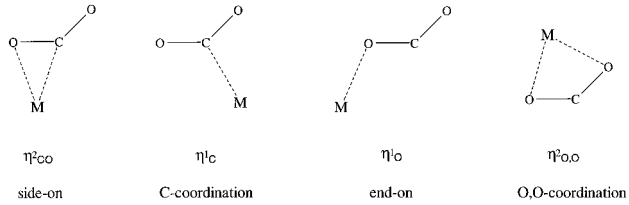

Figure 4. Coordination modes in $Ni(CO_2)$

η^1_C and $\eta^2_{O,O}$ and the triplet state $\eta^2_{O,O}$ are transition states, as indicated by the imaginary frequencies. The optimization procedure for the η^1_C isomer in its triplet state yielded a η^2_{CO} geometry with parameters slightly different from those calculated with the η^2_{CO} initial geometry. The discrepancies between the two entries in Table 3 indicate the numerical uncertainty associated with the various properties due to the incompleteness of the integration grid. Comparing the calculated properties of the coordinated CO_2 ligand with those of the free CO_2 molecule (see footnote in Table 3), we see that CO_2 is only slightly distorted in the η^1_O coordination, whereas it undergoes significant structural changes in all of the other cases.

In order to verify that the side-on structure is the global minimum on the singlet PES, we derived two potential energy curves corresponding to the $\eta^2_{CO} \rightarrow \eta^1_C$ and $\eta^2_{CO} \rightarrow \eta^1_O$ transitions (Figures 5 and 6). Although the geometry of the CO_2 was not allowed to relax in these calculations and the R(NiC) and R(NiO) parameters were not varied, the two potential energy curves clearly show that the energy monotonically increases when going from the side-on to either the η^1_C or the η^1_O coordinations. It is therefore very likely that the η^2_{CO} structure is the global minimum.

V.2. The $Ni(CO_2)(N_2)_n$ (n = 1, 2) Complexes. Two different mixed N_2/CO_2 complexes, $Ni(CO_2)(N_2)$ and $Ni(CO_2)(N_2)_2$, were considered in modelling the effect of dinitrogen molecules on the complexation of CO_2. Based on the unambiguous stability of the η^2_{CO} isomer in the case of the binary $Ni(CO_2)$ complex and the similarity in the frequencies of the observed IR bands in neat CO_2 and N_2 matrices, we assumed a side-on CO_2 coordination in both mixed complexes and fully optimized their geometries. Actually, calculations showed that in end-on $Ni(CO_2)(N_2)$, the CO_2 moiety becomes linear and cannot afford such vibrational frequencies. The equilibrium structures of $Ni(CO_2)(N_2)$ and $Ni(CO_2)(N_2)_2$ are shown in Figure 7, and the optimized parameters are given in Table 4 along with those of the singlet η^2_{CO} $Ni(CO_2)$ complex.

Both complexes are nearly planar with roughly linear N_2 coordination. The slight deviation from nonplanarity is probably due to the grid effect. The CO_2 coordination in the mixed complexes is very similar to that in η^2_{CO} $Ni(CO_2)$; however, the CO_2 ligand appears to be a bit less distorted with respect to free CO_2 than in the binary complex. Consequently, the CO stretching frequencies are shifted toward higher values by 50−70 cm^{-1} as compared to those in η^2_{CO} $Ni(CO_2)$, but interestingly, the OCO bending frequency is hardly affected by the N_2 coordination. The effect of the second N_2 molecule on the CO_2 coordination seems to be less important: the CO bond lengths vary by less than 0.01 Å, the OCO valence angle varies by less than one degree, and there is only about a 10 cm^{-1} shift in the CO_2 frequencies when going from $Ni(CO_2)(N_2)$ to $Ni(CO_2)(N_2)_2$.

VI. Discussion

VI.1. The $Ni(CO_2)$ Complex. Based on the electronic spectra, we know that there are no metallic aggregates present in our deposits and that carbon dioxide spontaneously reacts with nickel. Nevertheless, the reaction yield is very low, as

TABLE 3: Relative Stabilities, Optimized Geometries and IR Spectra of Various Structures of $Ni(CO_2)$[a]

	η^2_{CO}		η^1_C		η^1_O		η^3_{OCO}	
	singlet	triplet	singlet	triplet[b]	singlet	triplet	singlet	triplet
ΔE	0.0	14.8	17.8	15.1	23.8	20.5	49.3	37.2
R(NiC)	1.823	1.945	1.759	1.953			2.294	2.223
R(NiO)	1.826	2.163		2.195	1.744	2.737	1.802	2.039
$R(CO^1)$	1.288	1.248	1.237	1.244	1.186	1.181	1.240	1.256
$R(CO^2)$	1.201	1.202	1.237	1.202	1.184	1.175	1.240	1.255
α(OCO)	144.6	149.3	151.2	149.8	179.0	179.8	103.3	130.0
α(NiOC)					176.5	139.2		
ω_1	1901(539)	1947(384)	1830(532)	1953(379)	2365(661)	2363(753)	1118(55)	1613(337)
ω_2	1087(99.0)	1154(239)	1169(260)	1161(236)	1264(270)	1314(1.4)	775(22)	1185(172)
ω_3	702(129)	607(398)	808(161)	596(406)	379(9.5)	618(21)	570(87)	631(96)
ω_4	532(0.9)	514(1.7)	507(3.7)	510(1.1)	349(8.4)	609(15)	499(5.7)	256(10)
ω_5	523(2.5)	298(0.5)	322(25)	282(0.3)	346(7.4)	90(1.2)	346(5.1)	234(31)
ω_6	284(4.2)	162(4.1)	i304	137(4.1)	219(0.2)	62(1.2)	i578	i463

[a] Units: bond lengths in Å, angles in degrees, and energies (with respect to sing η^2_{CO}) in kcal/mol. The calculated equilibrium parameters for free CO_2 are: R(CO) = 1.177 Å, ω_1 = 2374(601), ω_2 = 1321(0), ω_3 = 630(25) cm^{-1}. [b] Geometry optimization from a η^1_C initial geometry yields η^2_{CO} structure. Optimized parameters of the obtained η^2_{CO} structure are given to illustrate the numerical uncertainty due to the incompleteness of the integration grid.

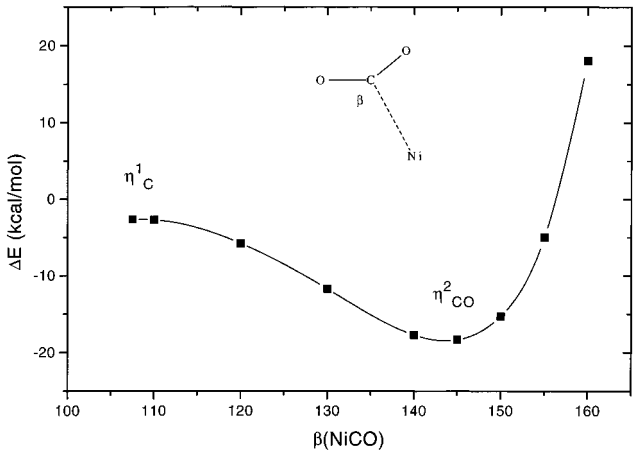

Figure 5. The $\eta^2_{CO} \rightarrow \eta^1_C$ potential energy curve. All parameters fixed ($R(CO^1) = R(CO^2)$ = 1.24 Å, α(OCO) = 145°, and R(NiC) = 1.8 Å), except the β(NiCO) angle, which was varied between 107.5° and 160°.

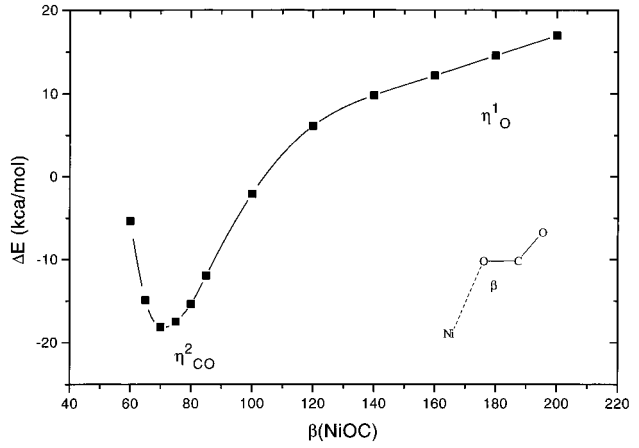

Figure 6. The $\eta^2_{CO} \rightarrow \eta^1_O$ potential energy curve. All paremeters fixed ($R(CO^1) = R(CO^2)$ = 1.24 Å, α(OCO) = 145°, and R(NiO) = 1.8 Å), except the β(NiOC) angle, which was varied between 60° and 200°.

even in neat CO_2 matrices, we can observe metal atom transitions. It is probable that the reaction takes place in the gas phase rather than in the matrix at 10 K. We also conclude that nickel atoms do not react easily with CO_2, as bands observed for complexes in dilute matrices are very weak and do not grow upon annealing.

Infrared spectra confirm the low yield of reaction of nickel toward CO_2 since the maximum absorption of the most intense bands is about 10%. All the observed frequencies are in the ranges expected for coordinated CO_2, although the ν(C═O) modes are usually located at lower wavenumbers than 1800 cm^{-1}. The band shapes, annealing experiments, and isotopic shifts showed that two different species are formed, both of them with a 1:1 stoichiometry: $Ni(CO_2)$.

Because annealing did not induce changes in the spectra attributable to site effects, we can conclude that both sets of bands arise more likely from structurally different complexes rather than from similar species condensed in different matrix sites.

The theoretical results suggest that the CO_2 coordination in the $Ni(CO_2)$ complex is side-on, all other isomers being much less stable. Since the predicted vibrational frequencies for the singlet state η^2_{CO} complex are fairly close to the observed frequencies (for instance, the average percentage deviation from the 1815, 1131, and 744 cm^{-1} values observed for A is less than 5%), we can reasonably conclude that the most abundant

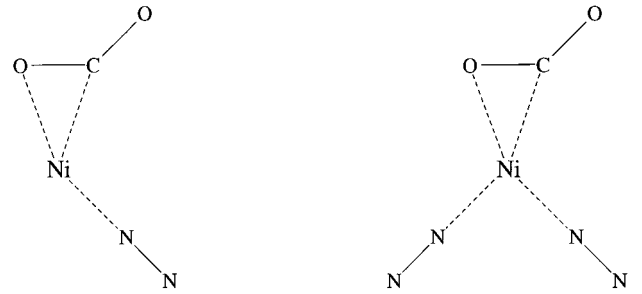

Figure 7. Equilibrium structure of the $Ni(CO_2)(N_2)$ and $Ni(CO_2)(N_2)_2$ complexes.

TABLE 4: Calculated Properties for $Ni(CO_2)(N_2)$ and $Ni(CO_2)(N_2)_2$[a]

	$Ni(CO_2)(N_2)$	$Ni(CO_2)(N_2)_2$	$Ni(CO_2)$
R(NiC)	1.890	1.924	1.823
R(NiO)	1.855	1.910	1.826
R(C−O)	1.269	1.263	1.288
R(C═O)	1.194	1.199	1.201
α(OCO)	149.3	148.4	144.6
R(NiN)	1.731	1.774/1.892[b]	
R(NN)	1.133	1.129/1.125	
α(NiNN)	176.1	175.3/165.1	
α(CNiN)		108.7/141.5	
α(NNiN)		108.4	
ω_1 (asym CO str)	1975(568)	1965(571)	1901(539)
ω_2 (sym CO str)	1132(177)	1145(193)	1087(99)
ω_3 (OCO bend)	701(176)	689(257)	702(129)

[a] Same units as in Table 3. [b] The first and second numbers refer to the right and left side NiN_2 units, respectively (see Figure 7).

TABLE 5: Calculated Harmonic Frequencies and Force Constants of the Side-on $NiCO_2$ Complex and Its Labeled Derivatives from Normal Coordinate Analysis (NCA) and DFT Calculations at the B/P-B_1^{num} Level[a]

	Ni(CO_2)[b]		Ni($C^{18}O_2$)[c]			Ni($^{13}CO_2$)[c]			
	NCA	exptl	NCA	DFT	exptl	NCA	DFT	exptl	force constants[d]
ν(C═O)	1815	1815	31	34	40	50	50	42	11.2 (10.0)
ν(C-O)	1137	1131	42	48	18	14	9	15	7.5 (6.2)
δ(OCO)	744	744	23	21	28	14	13	14	0.88 (1.05)
ν(NiO)	399	410	17	15	10	1	5	0	1.0 (0.95)
γ(C═O)	588[e]		6	6		17	15		0.64 (0.64)
ν(NiC)	312		12	10		2	2		1.0 (1.0)

[a] Wavenumbers and isotopic shifts are given in cm^{-1}, force constants in mdyn·Å^{-1} for bonds, mdyn·Å·rad^{-2} for angles, and mdyn·rad^{-1} for bond−angle interactions. [b] Wavenumbers in cm^{-1}. [c] Isotopic shifts in cm^{-1}. [d] Initial values taken from $Ni(PCy_3)_2(CO_2)$[25] are given in parentheses. Bond-angle interaction force constants are: $f(\nu_{C=O},\nu_{CO}) = 0.81$, $f(\nu_{C=O},\delta_{OCO}) = 0.4$, and $f(\nu_{CO},\delta_{OCO}) = 0.3$. [e] The out-of-plane bending mode has not been fitted.

1:1 complex (A), observed in neat CO_2 matrices, is the singlet state η^2_{CO} Ni(CO_2). The calculated IR intensities are also in line with the observed spectra. The band corresponding to the asymmetric stretching ν(C═O) is the most intense, and the symmetric stretching ν(CO) and bending δ(OCO) bands have similar intensities.

We note that the frequencies predicted for the singlet η^1_C isomer match the observed values slightly better, and the splitting of the CO stretching frequencies ($\Delta\omega_{CO} = \omega_{C=O} - \omega_{C-O}$) is much closer to the experimental values (684 cm^{-1} for A and 624 cm^{-1} for B) for the η^1_C case (661 cm^{-1}) than for η^2_{CO} (814 cm^{-1}). However, given the substantial difference in the stability of the two forms (η^1_C is about 18 kcal/mol above η^2_{CO}), it is unlikely that C-coordination, which is in fact a transition state, is stabilized by the matrix. An additional argument against the C-coordination is that, as shown in our previous studies,[35] the C-coordination induces a smaller split in the ν(CO) stretching frequencies (less than 500 cm^{-1}) compared to those induced by either η^2_{CO} or η^1_O coordinations. This also means that the DFT calculations probably overestimate $\Delta\omega_{CO}$ for both η^2_{CO} and η^1_C isomers.

We should also keep in mind that the calculations do not take into account the "matrix" effect; they describe gas phase molecules. If argon matrices can be considered as "good" matrix media (weak matrix−molecule interaction), neat carbon dioxide matrices can induce stronger effects on the isolated species, leading to larger frequency shifts, especially of the asymmetric stretching mode ν(C═O), which is very sensitive to polar effects. Compared to the gas phase or a noble gas matrix, the frequency is then lowered, as is usually observed for carbonyl compounds in polar solvents.[36]

Previous studies[2,35,37,38] allowed us to correlate the structure of CO_2 complexes with their spectroscopic properties, especially with the help of isotopic labeling.

First, the CO stretching modes splitting and the OCO bending frequency are known to be related to the value of the OCO angle in the complex. In fact, the correlation can be made for any nonlinear triatomic molecule XY_2.[39] For example, in $(PCy_3)_2Ni(CO_2)$,[25,40] a side-on complex for which ν(CO) splitting is 591 cm^{-1}, the OCO angle is 136°. In our case, the OCO angle is calculated to be 149° for species A and must lie between 136 and 149° for species B. Note that DFT predicts $\alpha = 145°$ for the ground state η^2_{CO} molecule.

Next, end-on coordination induces, in both CO stretching modes, a larger total isotopic shift when the oxygen is isotopically substituted ($^{16/18}$O, namely, 70 cm^{-1}) than when the carbon is ($^{12/13}$C, about 60 cm^{-1}), whereas the values are expected to be equal (about 60 cm^{-1}) for side-on coordination. In our case, the $^{12/13}$C and $^{16/18}$O effects are respectively 59 and 65 cm^{-1} for species A and 58 and 68 cm^{-1} for species B. These results lead us to favor an end-on coordination for species B and a side-on geometry for A. But an end-on coordination for B is inconsistent both with a smaller OCO angle and our DFT calculations. So, we propose that B, which has stronger interactions with the surrounding CO_2 molecules of the matrix, as outlined by broader bands in the FTIR spectrum, has a side-on structure with an OCO angle of 140°.

In order to derive a harmonic force field for the Ni(CO_2) complex, we performed a normal coordinate analysis (NCA) and force constant refinement, using the experimental IR data for species A. The structural data were taken from our DFT results (see Table 3) and the initial force constants were those obtained from our previous normal coordinate analysis on $(PCy_3)_2Ni(CO_2)$ [25].

Table 5 summarizes the final force constants and the calculated frequencies, along with the experimental and DFT data. It is seen that both NCA and DFT results reproduce relatively well the experimental isotopic shifts, except the ^{18}O shift of the ν(CO) mode where both theoretical approaches yield a considerably larger shift than the experimental value of 18 cm^{-1}. We have tried to vary the OCO angle and the force constants in the NCA, but it turned out that this isotopic shift was rather insensitive to these variations. We think that the discrepancy between the experimental and theoretical isotopic shifts is probably due to an inaccurate experimental value (the poor quality of the $NiC^{18}O_2$ IR spectrum, especially the weakness of the bands, prevented us from unambiguously assigning the $\nu(C^{18}O)$ mode).

Comparison of the force fields for Ni(CO_2) and $(PCy_3)_2$Ni(CO_2)[25] shows that, the OCO angle being larger (149°) in Ni(CO_2) than in the phosphine complex (136°), the C═O bonds retains more "double bond" character in Ni(CO_2) and the force constants of ν(C═O) and ν(CO) are slightly higher, being respectively increased by 12 and 20%.

We will now consider the bonding in the η^2_{CO} Ni(CO_2) molecule.

The 13 valence electrons in the ground state (^{1}A′)η^2_{CO} Ni(CO_2) molecule are associated with nine a′ and four a″ doubly occupied molecular orbitals. The ordering and the approximate description of these orbitals are as follows: 1a′(4σ)2a′(5σ)3a′(6σ)4a′(7σ)5a′(1π)1a″(1π)6a′(2π+3d)2a″(3d)7a′(3d+3π*)8a′(3d+4s)3a″(3d)4a″(3d)9a′(3d+4s), where σ and π denote CO_2 orbitals and 3d and 4s are Ni orbitals. Among the CO_2 orbitals, 2π is the highest lying occupied CO_2 orbital localized on the two O atoms (lone pairs), whereas 3π* is the first virtual CO_2 orbital. It is an antibonding combination of the pπ carbon and oxygen atomic orbitals.

Most of the Ni(CO_2) orbitals are pure CO_2 or Ni orbitals with only a slight (usually about 5%) admixture with the other moiety; however, the 6a′ and 7a′ orbitals are mixtures of metal and ligand orbitals (see Figure 8). The former is composed of 17% Ni (3d) and 83% CO_2, the latter has 55% Ni (predominantly 3d) and 45% CO_2. The CO_2 contributions to 6a′ and 7a′ have essentially 2π and 3π* character respectively, so one

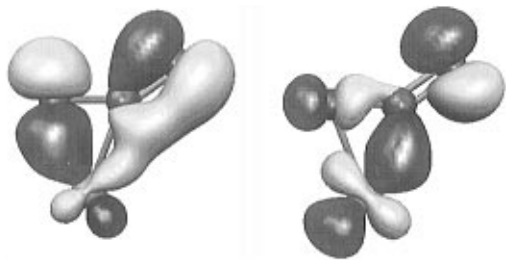

Figure 8. Metal−ligand bonding orbitals (6a′ and 7a′) in η^2_{CO} Ni(CO$_2$).

TABLE 6: Net Mulliken Atomic Charges and Mayer Bond Orders for η^2_{CO} Ni(CO$_2$) and CO$_2$ Molecules

	Ni(CO$_2$)	CO$_2$
	Mulliken Charges	
Ni	+0.29	
O^{C-O}	−0.28	−0.18
C	+0.17	+0.36
O$^{C=O}$	−0.18	−0.18
	Mayer Bond Orders	
NiC	0.81	
NiO	0.66	
C−O	1.38	2.18
C=O	2.03	2.18

can say that 6a′ corresponds to a $CO_2 \rightarrow$ Ni, while 7a′ to a Ni $\rightarrow CO_2$ charge transfer, indicating that the Ni−CO$_2$ bond can be viewed as a dative π bond, just as in Ni(C$_2$H$_4$) or NiCO. Since the charge donation from the metal to CO$_2$ is considerably larger than that in the opposite direction, the Ni atom has a net positive charge and the CO$_2$ ligand has an anionic character (see Table 6). Because of the partial occupation of the $3\pi^*$ CO$_2$ orbitals in the complex, the CO bonds (and especially the ones interacting directly with the Ni atom) are weakened as seen from the calculated bond orders (also given in Table 6) or from the shifts in the CO$_2$ frequencies upon coordination.

The hybridization of the 3d and 4s orbitals (8a′ and 9a′) polarizes the Ni s electrons away from the ligand in order to reduce the Pauli repulsion between the 4s and the occupied CO$_2$ orbitals. The hybridization involves the Ni 4p orbitals as well, resulting in a nonnegligible 4p Ni population in the complex (the electron configuration of the nickel atom is $3d^{8.98}4s^{0.61}$-$4p^{0.12}$). The first virtual orbital (10a′) of the ^{1}A′ η^2_{CO} Ni(CO$_2$) complex lies about 1.2 eV above 9a′ and it is a Ni sdp hybrid with about 20% CO$_2$ character. In the triplet state η^2_{CO} Ni(CO$_2$) 10 a′ becomes singly occupied, and because of its Ni−CO$_2$ antibonding nature, the triplet state is significantly less stable than the singlet state.

The binding energy of the ground state side-on complex is calculated to be $D_0 = 21.1$ kcal/mol. Assuming the same BSSE as we obtained for the Ni(C$_2$H$_4$) molecule[41] and correcting D_0 for this error, we get 17.5 kcal/mol for the binding energy. This is about half the value calculated for Ni(C$_2$H$_4$), showing that despite the similarities in the bonding in the two complexes, Ni(CO$_2$) is thermodynamically far less stable than Ni(C$_2$H$_4$), which might be one of the reasons that CO$_2$ gives a considerably lower yield upon complexation with Ni than C$_2$H$_4$ does.

It is interesting to mention here that a very similar binding energy (≈20 kcal/mol) was found for the Pd(CO$_2$) complex in a recent DFT study,[42] where the side-on coordination mode turned out to be the most stable as well. Among the other theoretically studied M(CO$_2$) species,[43−47] where M is a transition metal, only the Sc(CO$_2$) complex was predicted to have a similar stability (17 kcal/mol).[47] The Cu(CO$_2$),[43] Cr(CO$_2$),[44] and Ti(CO$_2$)[45] complexes were found to be very weakly bound, however, the binding energies for these systems were probably underestimated by the limited configuration interaction (CI) calculations.

VI.2. Role of Dinitrogen on CO$_2$ Coordination. As already mentioned in section VI.1, the reaction seems to take place in the gas phase, before condensation at 10 K on the cold window. Indeed, the mixed Ni/CO$_2$/N$_2$ complexes observed in the matrix exhibit no further reactivity by annealing up to 35 K and the only other compound formed is Ni(N$_2$)$_4$, which is a tetrahedral, stable, and unreactive saturated complex.[28,29]

Taking into consideration the very high reactivity of N$_2$ toward nickel compared to that of CO$_2$, it is reasonable to assume that CO$_2$ reacts with unsaturated Ni(N$_2$)$_n$ species ($n < 4$), yielding mixed CO$_2$/N$_2$ complexes which are stable enough to keep CO$_2$ coordinated in a dinitrogen matrix environment. The most probable stoichiometry is then Ni(CO$_2$)(N$_2$)$_n$ with $n = 1$ or 2 as CO$_2$ is side-on coordinated to the nickel atom.

The theoretical results obtained for the Ni(CO$_2$)(N$_2$) and Ni(CO$_2$)(N$_2$)$_2$ complexes support the formation of mixed complexes in that the CO stretching frequencies are blue shifted and the OCO bending frequency is red shifted in the mixed complexes relative to those in the binary complex, as observed experimentally. However, we are still unable to specify the number of coordinated N$_2$ molecules in the mixed species, even if we assume a side-on coordination and compare the theoretical frequencies to those of the most abundant species (C). On the other hand, we can look at the energetics of the coordination of CO$_2$ to the different Ni(N$_2$)$_n$ species, which are presumably formed prior to CO$_2$ coordination because of the excess N$_2$. From the data listed in Table 1, we get 32.2 and 3.5 kcal/mol for the energies of the Ni(CO$_2$)(N$_2$) $\rightarrow$ Ni(N$_2$) + CO$_2$ and Ni(CO$_2$)(N$_2$)$_2$ $\rightarrow$ Ni(N$_2$)$_2$ + CO$_2$ reactions, respectively, indicating that the CO$_2$ coordination to Ni(N$_2$) is thermodynamically favored over its coordination to a ground state Ni atom, whereas the coordination to Ni(N$_2$)$_2$ is very unlikely. The low CO$_2$ binding energy obtained for Ni(CO$_2$)(N$_2$)$_2$ is due to the fact that the equilibrium structure of the Ni(N$_2$)$_2$ molecule is linear and the bending of this unit upon the CO$_2$ coordination requires a considerable amount of energy. The bent Ni(N$_2$)$_2$ molecule with R(NiN) = 1.750 Å, R(NN) = 1.138 Å (values in linear Ni(N$_2$)$_2$) and with α(NNiN) = 108.4° (angle in Ni(CO$_2$)(N$_2$)$_2$) is 17 kcal/mol above the linear complex.

In order to understand the increased CO$_2$ binding energy in Ni(CO$_2$)(N$_2$) versus Ni(CO$_2$), we calculated the potential energy curves corresponding to the interaction of the s^1d^9 (^{3}D) Ni atom and the singlet Ni(N$_2$) molecule with a gas phase (linear) CO$_2$ molecule, as shown in Figure 9. The difference in the shape of the two curves is quite striking. The Ni−CO$_2$ interaction appears to be repulsive, while the interaction energy for Ni(N$_2$)−CO$_2$ continuously decreases when approaching CO$_2$, reaching a minimum at around $y = 2.0$ Å, where ΔE is about 7 kcal/mol. The Ni(N$_2$) orbitals reveal that the coordination of N$_2$ to Ni atom induces a hybridization of the Ni 4s and 3d orbitals and, as a result, the electron configuration of the Ni atom in Ni(N$_2$) becomes very similar to that in Ni(CO$_2$) ($4s^{0.79}$-$3d^{9.02}4p^{0.02}$ in Ni(N$_2$) and, as we saw earlier, $4s^{0.61}3d^{8.98}4p^{0.12}$ in Ni(CO$_2$)). Consequently, the s electrons on the Ni atom are already polarized away from the approaching CO$_2$, allowing the metal d_π orbitals to interact with the CO$_2$ $3\pi^*$ orbitals. Since the metal $\rightarrow$ ligand charge transfer is not great in Ni(N$_2$) (0.16 e), the Ni atom in Ni(CO$_2$)(N$_2$) can still donate a similar amount of charge to the CO$_2$ as in Ni(CO$_2$) (0.25 e vs 0.30 e). Since the 4s−3d hybridization energy cost has already been paid in coordinating with N$_2$, the CO$_2$ binding energy is higher in Ni(CO$_2$)(N$_2$) than in Ni(CO$_2$). This is a clear demonstration of the important role of cooperative effect in metal−ligand

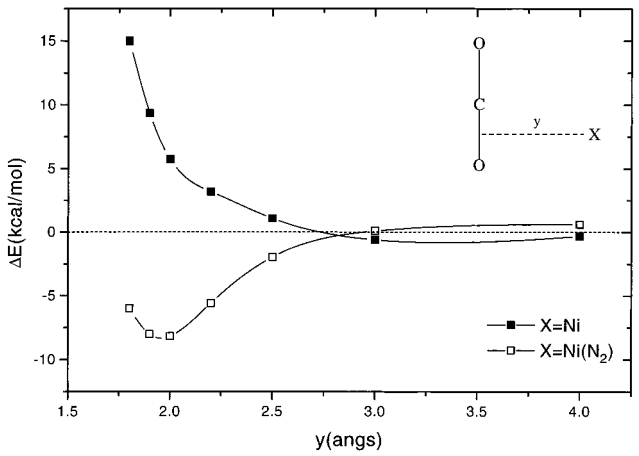

Figure 9. Interaction of the s^1d^9 (^3D) Ni atom and the singlet state $Ni(N_2)$ molecule with a linear CO_2 molecule. The geometry of the CO_2 molecule and the $Ni(N_2)$ complex are fixed at their equilibrium structures (see Table 1) and the distance between the midpoint of the CO bond and the Ni atom is varied. For $CO_2 + Ni(N_2)$, the molecular axes of CO_2 and $Ni(N_2)$ are perpendicular.

association reactions, which has already been observed for other systems as well.[48]

VII. Conclusion

FTIR and UV−visible studies have shown that two structurally slightly different $Ni(CO_2)$ complexes are trapped in neat CO_2 matrices at 10 K. The gas phase $Ni(CO_2)$ molecule has been fully characterized by normal coordinate analysis and density functional calculations with nonlocal corrections. The binding energy of 18 kcal/mol shows that this complex is far less stable than "similar" molecules, like $Ni(C_2H_4)$ or NiCO. The CO_2 coordination mode is found to be side-on, and the OCO angle (145°) is larger than usually encountered in stable side-on CO_2 complexes. The reaction yield for the reaction between Ni and CO_2 is very low and no reaction occurs in argon dilute matrices. Interestingly, the coordination of CO_2 is promoted by using N_2 in place of rare gas matrices. This has been rationalized by the difference in CO_2 binding energies obtained for $Ni(CO_2)(N_2)$ and $Ni(CO_2)$ complexes.

This study illustrates the important roles played by the matrix and the cooperative effects of coligands in binding molecules to metal atoms.

Further work on similar systems ($Ni/CO_2/C_2H_4$) is in progress.

Acknowledgment. J.M. and I.P. acknowledge financial support from CNRS and the Hungarian Academy of Sciences. I.P. also acknowledges support from OTKA (Grant TO2O231). J.M. is pleased to thank Prof. M. Moskovits for critical reading of the manuscript.

References and Notes

(1) Behr, A. *Carbon Dioxide Activation by Metal Complexes*; VCH: Weinheim, Germany, 1988.
(2) Mascetti, J.; Tranquille, M. *J. Phys. Chem.* **1988**, *92*, 2177.
(3) Aresta, M.; Quaranta, E.; Tommasi, I. *New J. Chem.* **1994**, *18*, 133.
(4) Braunstein, P.; Matt, D.; Nobel, D. *Chem. Rev.* **1988**, *88*, 747.
(5) Fournier, R.; Pápai, I. *Recent Advances in Computational Chemistry*, Part I, Chong, D., Ed.; World Scientific: Singapore, 1995.
(6) (a) Cossé-Mertens, C. Thesis, Université Bordeaux I, 1981. (b) Galan, F. Thesis, Université Bordeaux I, 1994.
(7) Tranquille, M. *Spectra 2000* **1984**, *98*, 43.
(8) Sambe, H.; Felton, R. H. *J. Chem. Phys.* **1975**, *62*, 1122.
(9) Dunlap, B. I.; Conolly, J. W. D.; Sabin, J. R. *J. Chem. Phys.* **1979**, *71*, 3396.
(10) Andzelm, J.; Radzio, E.; Salahub, D. R. *J. Chem. Phys.* **1985**, *83*, 4573.
(11) Fournier, R.; Andzelm, J.; Salahub, D. R. *J. Chem. Phys.* **1989**, *90*, 6371.
(12) Salahub, D. R.; Fournier, R.; Mlynarski, P.; Pápai, I.; St-Amant, A.; Ushio, J. *Density Functional Methods in Chemistry*; Labanowski, J.; Andzelm, J., Eds.; Springer-Verlag: New York, 1991, p 77.
(13) St-Amant, A.; Salahub, D. R. *Chem. Phys. Lett.* **1990**, *169*, 387.
(14) St-Amant, A. Ph.D. Thesis, Université de Montréal, 1991.
(15) Daul, C.; Goursot, A.; Salahub, D. R. *Numerical Grid Methods and Their Application to Schrödinger's Equation*; Cerjan, C., Ed.; NATO ASI Series; Kluwer Academic Press: Boston, 1993; Vol. 412, p 153.
(16) Becke, A. D. *Phys. Rev. A.* **1988**, *38*, 3098.
(17) Slater, J. C. *Quantum Theory of Molecules and Solids, Vol. 4: The Self-Consistent Field for Molecules and Solids*; McGraw-Hill: New York, 1994.
(18) Perdew, J. P. *Phys. Rev. B.* **1986**, *33*, 8822; erratum in *Phys. Rev. B.* **1986**, *38*, 7406.
(19) Godbout, N.; Andzelm, J.; Salahub, D. R.; Wimmer, E. *Can. J. Chem.* **1992,** *70*, 560.
(20) Sim, F.; Salahub, D. R.; Chin, S.; Dupuis, M. *J. Chem. Phys.* **1991**, *95*, 4317.
(21) Pápai, I. *J. Chem. Phys.*, **1995**, *103*, 1860.
(22) Pulay, P. *Applications of Electronic Structure Theory, Modern Theoretical Chemistry*; Schaefer, H. F., III, Ed.; Plenum: New York, 1977; Vol. 4.
(23) Komornicki, A.; McIver, J. W. *J. Chem. Phys.* **1979**, *70*, 2014.
(24) Schachtschneider, J. H.; Snyder, R. G. *Spectrochim. Acta* **1963**, *19*, 117.
(25) Jegat, C.; Fouassier, M.; Tranquille, M.; Mascetti, J.; Tommasi, I.; Aresta, M.; Igold, F.; Dedieu, A. *Inorg. Chem.* **1993**, *32*, 1279.
(26) Schroeder, W.; Grinter, R.; Schrittenlacher, W.; Rotermund, H. H.; Kolb, D. M. *J. Chem. Phys.* **1985**, *82*, 1623.
(27) Moskovits, M.; Hulse, J. E. *J. Chem. Phys.* **1977**, *66*, 3988.
(28) Huber, H.; Kundig, E. P.; Moskovits, M.; Ozin, G. A. *J. Am. Chem. Soc.* **1973**, *95*, 332.
(29) Klotzbucher, W.; Ozin, G. A. *J. Am. Chem. Soc.* **1975**, *97*, 2672.
(30) Becker, A.; Langel, W.; Maass, S.; Knoezinger, E. *J. Phys. Chem.* **1993**, *97*, 5525.
(31) Manceron, L.; Hawkins, M.; Andrews, L. *J. Phys. Chem.* **1986**, *90*, 4987.
(32) De Kock, R. L. *Inorg. Chem.* **1971**, *10*, 1205.
(33) Kundig, E. P.; Moskovits, M.; Ozin, G. A. *Can. J. Chem.* **1973**, *51*, 2737.
(34) Eischens, R. P. *Spectrochim. Acta* **1965**, *21*, 1295.
(35) Jegat, C.; Mascetti, J. *New J. Chem.* **1991**, *15*, 17.
(36) Nakamoto, K. *Infrared Spectra of Inorganic and Coordination Compounds*, 4th ed.,Wiley-Interscience: New-York, 1986.
(37) Jegat, C.; Fouassier, M.; Mascetti, J. *Inorg. Chem.* **1991**, *30*, 1521.
(38) Jegat, C.; Fouassier, M.; Tranquille, M.; Mascetti, J. *Inorg. Chem.* **1991**, *30*, 1529.
(39) Herzberg, G. *Infrared and Raman Spectra of Polyatomic Molecules*, 7th ed., D. van Nostrand Comp.: New York, 1956.
(40) Dohring, A.; Jolly, P. W.; Kruger, C.; Romao, M. J. *Z. Naturforsch.* **1985**, *40B*, 484.
(41) The BSSE for $Ni(C_2H_4)$ was estimated to be 3.6 kcal/mol (see: Pápai, I.; Mink, J.; Fournier, R.; Salahub, D. R. *J. Phys. Chem.* **1993**, *97*, 9986). It is quite reasonable to assume a similar error for the side-on $Ni(CO_2)$ complex since (i) the R(NiC) and R(NiO) distances in $Ni(CO_2)$ are similar to R(NiC)'s in $Ni(C_2H_4)$ and ii) both calculations were carried out by using the same functional and the same basis sets.
(42) Sirois, S.; Castro, M.; Salahub, D. R. *Int. J. Quant. Chem.* **1994**, *S28*, 645.
(43) Caballol, R.; Marcos, E. S.; Barthelat, J. *J. Phys. Chem.* **1987**, *91*, 1328.
(44) Jeung, G. H. *Mol. Phys.* **1988**, *65*, 669.
(45) Jeung, G. H. *Mol. Phys.* **1989**, *67*, 747.
(46) Jeung, G. H. *Chem. Phys. Lett.* **1995**, *232*, 319.
(47) Sodupe, M.; Branchadell, V.; Oliva, A. *J. Phys. Chem.* **1995**, *99*, 8567.
(48) Sunil, K. K. *Chem. Phys. Lett.* **1992**, *195*, 355.